Multiparticulate Drug Delivery Systems Preserve the Efficacy of Reduced-Dose Intermittent Benznidazole Therapy in Experimental Chagas Disease

Sebastian Del Rosso[1,2], Gastón Bergero[1,2], Yanina L. Mazzocco[1,2], Luciana Mezzano[3], Mónica García[4,5], Maria Pilar Aoki[1,2]

SUPPLEMENTARY MATERIAL

Electrocardiographic Recordings

Surface ECG was recorded using a non-invasive TM-300-V device (Temis Tech, Argentina) with a four-electrode configuration that digitally reconstructed the six limb leads (I, II, III, aVR, aVL, and aVF) through the EasyG acquisition software (Temis Tech, Argentina). Recordings were acquired at a paper speed of 50 mm/s and a sensitivity of 40 mm/mV, with filter settings of 1 Hz for baseline correction, 75 Hz for bandwidth limitation, and 40 Hz for muscle noise reduction. ECG analysis was performed offline and was qualitative rather than interval-based. Tracings were examined for abnormalities classically associated with experimental Chagas disease, including sustained rhythm disturbances, recurrent ectopic activity, gross atrioventricular or intraventricular conduction defects, abnormal QRS morphology, and consistent ST-T/repolarization abnormalities.

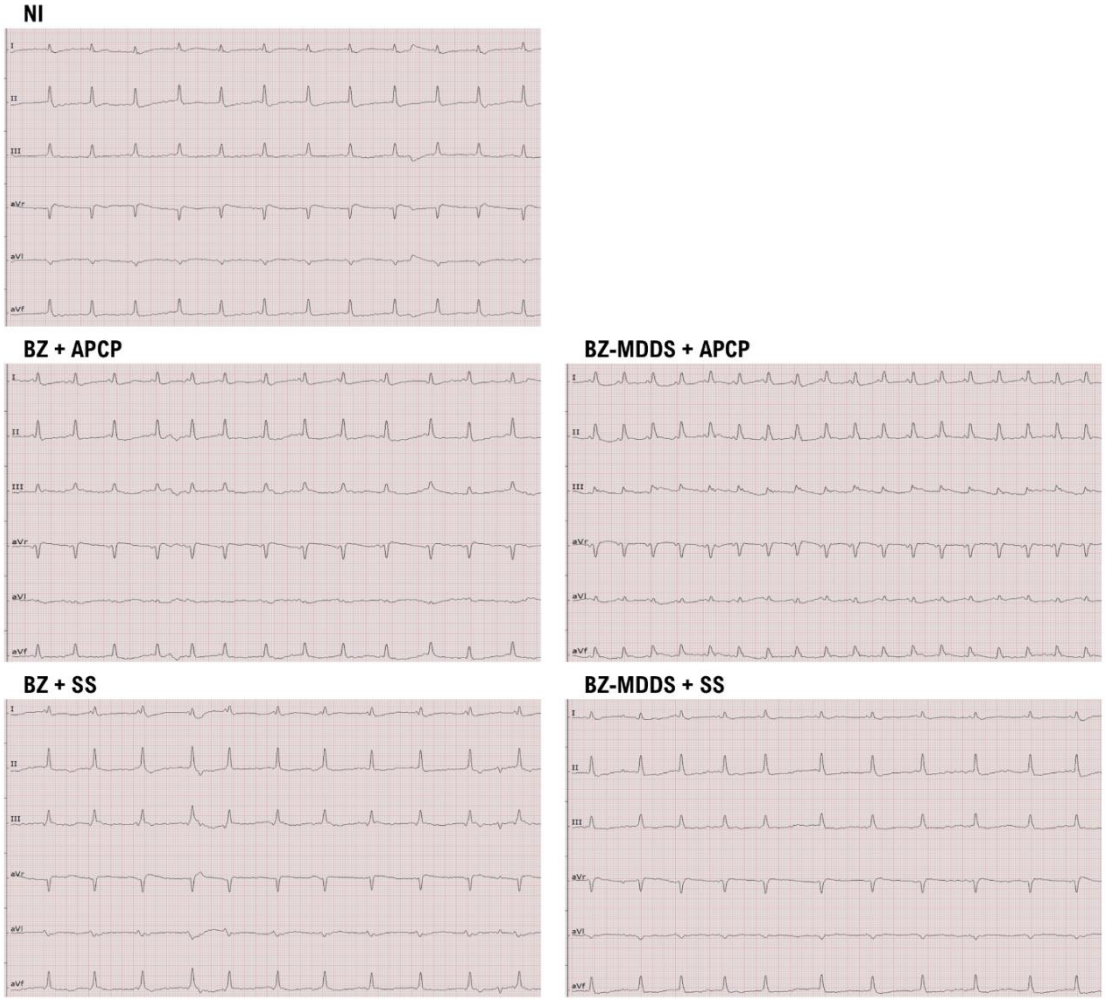

Supplementary Figure S1. **Representative samples of ECG registries recorded in experimental groups**. Surface ECG was recorded using a non-invasive device with a four-electrode configuration that digitally reconstructed the six limb leads (I, II, III, aVR, aVL, and aVF) through an acquisition software. Recordings were acquired at a paper speed of 50 mm/s and a sensitivity of 40 mm/mV, with filter settings of 1 Hz for baseline correction, 75 Hz for bandwidth limitation, and 40 Hz for muscle noise reduction. NI = Non-infected, MDDS = Multiparticulate drug delivery system, BZ = benznidazole, APCP = Adenosine 5′-(α,β-methylene)diphosphate.

Evaluation of TSKD14/Kd tetramer staining in BALB/c mice

As an additional exploratory readout of treatment response, we evaluated parasite-specific CD8+ T cells using MHC class I tetramers. This approach was based on previous work by Bustamante et al. (2008), who showed in experimental *T. cruzi* infection that effective benznidazole treatment was associated with contraction of parasite-specific CD8+ T-cell populations and a shift toward a central-memory phenotype. On that basis, we examined whether tetramer-based detection could be applied in our BALB/c model as a complementary immunological correlate of treatment efficacy.

To evaluate the feasibility of tetramer-based detection of *T. cruzi*-specific CD8+ T cells in BALB/c mice, an MHC class I tetramer were obtained from the Tetramer Core Facility (TCF): TSKD14/Kd (*T. cruzi* trans-sialidase 327–336, IYNVGQVSI, BV421). Initial optimization focused on TSKD14/Kd staining in peripheral blood from BALB/c mice infected with 10^6 trypomastigotes and sampled at 10 dpi. Tetramer titration was performed using dilutions of 1:100, 1:300, 1:500, and 1:1000. The flow-cytometry panel included CD3 (AF488, eBioscience, Cat. No. 53-0031-82), CD8 (APC-Cy7, BioLegend, Cat. No. 100714), and Zombie Aqua viability dye (BioLegend, Cat. No. 423101). Based on titration results, a 1:300 dilution was selected for subsequent experiments. In a second experiment, eight-week-old male BALB/c mice were infected with 1,000 Tulahuen-strain trypomastigotes and treated with different benznidazole-based regimens, including free benznidazole, benznidazole-loaded multiparticulate drug-delivery systems, and pharmacological inhibition of CD73 with APCP. At 105 dpi, peripheral blood was collected to evaluate the frequency of TSKD14/Kd-positive CD8+ T cells as a potential immunological readout of treatment response. In addition, peripheral blood from a non-infected BALB/c mouse was included as a negative control for tetramer staining and is shown as a representative control in Supplementary Fig S2. The same antibody panel was used for these analyses.

TSKD14/Kd staining yielded similar proportions of tetramer-positive CD8+ T cells across the dilutions tested during the optimization step, supporting the use of a 1:300 dilution for subsequent analyses. However, when this approach was applied to peripheral blood samples obtained at 105 dpi from infected BALB/c mice subjected to the different treatment regimens, the frequency of TSKD14/Kd-positive CD8+ T cells was very low. The corresponding event counts were insufficient to support reliable downstream phenotypic analysis (Supplementary Fig S2). Therefore, under the present experimental conditions, tetramer-based evaluation could not be used as an informative endpoint for treatment response.

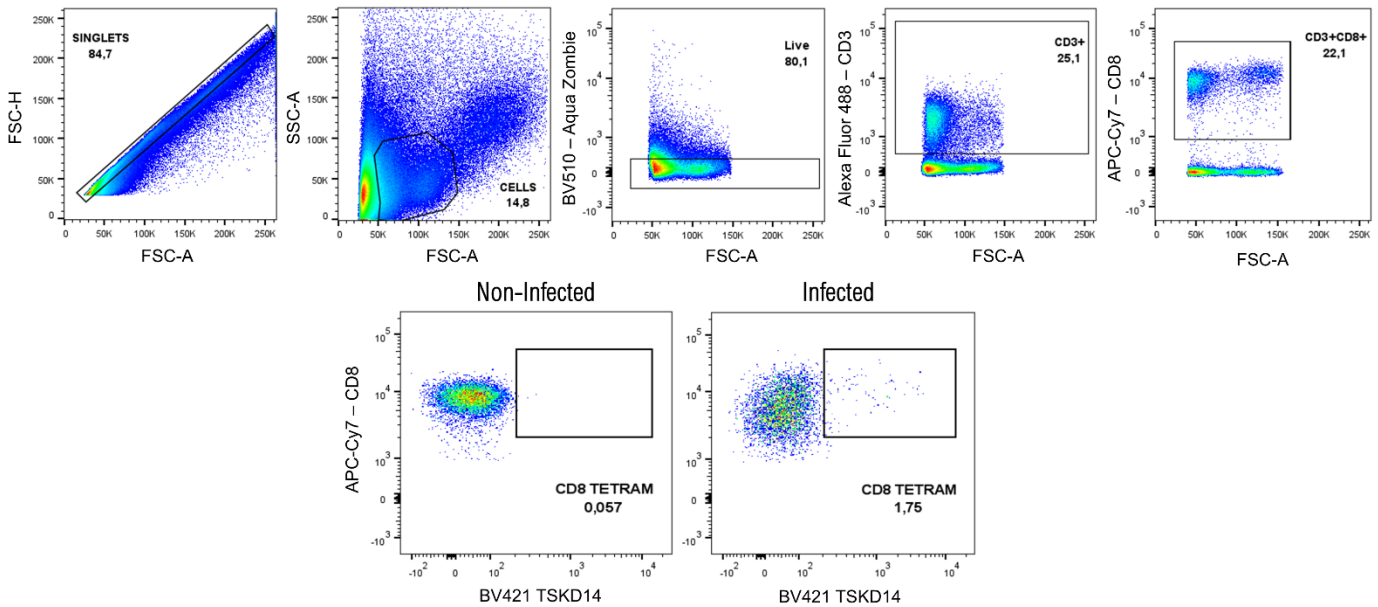

Supplementary Figure S2. Evaluation of TSKD14/Kd tetramer staining in BALB/c mice. Representative flow-cytometry analysis of peripheral blood cells stained with the TSKD14/Kd tetramer (*T. cruzi* trans-sialidase 327–336, IYNVGQVSI, BV421) in BALB/c mice. The upper panels show the gating strategy used to identify viable CD3+CD8+ T cells. The lower panels show representative dot plots from a non-infected mouse and an infected mouse, illustrating

the detection of TSKD14/Kd-positive CD8+ T cells. Tetramer staining was optimized in blood samples from BALB/c mice infected with 10^6 trypomastigotes at 10 dpi, and a 1:300 dilution was selected for subsequent experiments. When applied to peripheral blood collected at 105 dpi from mice infected with 1,000 Tulahuen-strain trypomastigotes and subjected to different treatment regimens, the frequency of tetramer-positive CD8+ T cells was very low, precluding reliable downstream phenotypic analysis.

Liver Histology and Inflammatory Indexes (Supplementary Table S1)

Livers were fixed in 10% buffered formalin and embedded in paraffin. Five-micron-thick sections were stained with hematoxylin-eosin. Photographs were taken using a Nikon Eclipse TE2000-U using a 20X objective. Inflammation was evaluated semi-quantitatively on low-power field (200X magnification) microscopic examination according to the distribution and extent of inflammatory foci (focal, confluent, or diffuse). Each tissue slide was analyzed for 10 random histological fields, and three different sections per mouse were examined. The presence of inflammatory cells, as well as morphological analysis of liver tissue damage was scored as – (absent), 1+ (focal), 2+ (mild), 3+(extensive inflammatory foci, minimal necrosis, and retention of tissue integrity), or 4+ (diffused inflammation with severe tissue necrosis, interstitial edema, and loss of integrity). Inflammatory infiltrates were characterized as diffused or focal depending upon how closely the inflammatory cells were located (Davies et al., 2014, Novaes et al., 2015). Histological assessment was performed blinded to treatment allocation

References

Bustamante, J. M., Bixby, L. M. & Tarleton, R. L. 2008. Drug-induced cure drives conversion to a stable and protective CD8+ T central memory response in chronic Chagas disease. *Nat Med,* 14**,** 542-50.

Davies, C., Dey, N., Negrette, O. S., Parada, L. A., Basombrio, M. A. & Garg, N. J. 2014. Hepatotoxicity in mice of a novel anti-parasite drug candidate hydroxymethylnitrofurazone: a comparison with Benznidazole. *PLoS Negl Trop Dis,* 8**,** e3231.

Novaes, R. D., Santos, E. C., Cupertino, M. C., Bastos, D. S., Oliveira, J. M., Carvalho, T. V., et al. 2015. Trypanosoma cruzi infection and benznidazole therapy independently stimulate oxidative status and structural pathological remodeling of the liver tissue in mice. *Parasitol Res,* 114**,** 2873-81.

Supplementary Table S1. Semi-quantitative determination of inflammatory foci as well as histological analysis of hepatic tissue damage. The analysis was performed at 120 dpi.

#	Sample	Inflammatory Infiltrate	Architecture Alterations	Necrosis	Steatosis	Fibrosis	Vessel Congestion	Observations
230Y	NI 1	-	-	-	2+	-	-	Conserved morphology
231Y	NI 2	-	-	-	2+	-	-	Conserved morphology
232Y	NI 3	-	-	-	2+	-	-	Conserved morphology
233Y	NI 4	-	-	-	-	-	-	Conserved morphology
234Y	NI 5	-	-	-	2+	-	-	Conserved morphology
235Y	BZ+APCP1	2+	2+	-	2+	-	-	Two amastigote nests. Mild Hepatocyte architecture alteration and mild steatosis
236Y	BZ+APCP2	1+	2+	2+	-	-	-	Mild hepatocyte architecture alteration and focal necrosis
237Y	BZ+APCP3	2+	-	-	-	-	-	One amastigote nest.
238Y	BZ+APCP4	1+	-	-	-	-	-	Slight dilation of sinusoidal spaces
239Y	BZ+APCP5	1+	-	1+	2+	-	-	Slight disorganization of lobular architecture
240Y	BZ+SS1	1+	-	-	-	-	2+	Vessel congestion
241Y	BZ+SS2	1+	-	-	2+	-	-	Conserved morphology
242Y	BZ+SS3	1+	-	-	2+	-	1+	One amastigote nest. Conserved morphology
243Y	BZ+SS4	2+	-	-	-	-	-	One amastigote nest. Conserved morphology
244Y	BZ+SS5	2+	-	-	-	-	1+	One amastigote nest. Slight vessel congestion
245Y	BZ-MDDS+APCP1	-	-	-	-	-	-	Conserved morphology
246Y	BZ-MDDS+APCP2	1+	-	-	2+	-	-	Conserved morphology. Hydropic changes in the hepatocyte cytoplasm
247Y	BZ-MDDS+APCP3	-	-	-	2+	-	-	Conserved morphology
248Y	BZ-MDDS+APCP4	1+	-	-	2+	-	-	Conserved morphology. Hydropic changes in the hepatocyte cytoplasm
249Y	BZ-MDDS+APCP5	1+	-	-	-	-	1+	Conserved morphology
250Y	BZ-MDDS+APCP6	1+	-	-	2+	-	-	Conserved morphology
251Y	BZ-MDDS+SS1	1+	-	-	2+	-	2+	Conserved morphology. Hydropic changes in the hepatocyte cytoplasm

252Y	BZ-MDDS+SS2	-	-	-	2+	-	-	Conserved morphology. Hydropic changes in the hepatocyte cytoplasm
253Y	BZ-MDDS+SS3	-	-	-	2+	-	-	Conserved morphology
254Y	BZ-MDDS+SS4	-	-	-	2+	-	-	Conserved morphology. Hydropic changes in the hepatocyte cytoplasm
255Y	BZ-MDDS+SS5	1+	-	-	-	-	-	Conserved morphology.
256Y	BZ-MDDS+SS6	1+	-	-	-	-	-	Conserved morphology.